Proceedings of HT2009
2009 ASME Summer Heat Transfer Conference
July 19-23, 2009, San Francisco, California USA

HT2009-88488

THERMAL RECTIFICATION BY BALLISTIC PHONONS IN ASYMMETRIC NANOSTRUCTURES

John Miller **Wanyoung Jang** **Chris Dames**

Department of Mechanical Engineering, University of California, Riverside CA 92521

ABSTRACT

In analogy to an electrical diode, a thermal rectifier transports heat more easily in one direction than in the reverse direction. Among various possible nanoscale rectification mechanisms, a ballistic rectifier relies on asymmetric scattering of energy carriers, as has been suggested for phonon transport in a sawtooth nanowire [S. Saha, L. Shi, & R. Prasher, IMECE 2006] or nanowire with special surface specularity function [N.A. Roberts and D.G. Walker, ITherm 2008]. We have used a Landauer-Buttiker method as well as a Monte Carlo method to model the asymmetric heat transport in such nanostructures, with careful attention to boundary conditions that satisfy the 2nd Law of Thermodynamics. The calculations show that ballistic rectification is only significant at relatively large "thermal bias," which causes significant anisotropy in the distribution function of energy carriers emitted at each of the two thermal contacts. We also propose experiments to observe this phenomenon using either phonons or photons.

1. INTRODUCTION

A thermal rectifier is the heat-transfer analogue of the familiar electrical diode: a two-terminal device that transmits heat more easily in one direction than in the reverse direction (Fig. 1). A familiar example is natural convection between two horizontal parallel plates: due to buoyancy, the heat transfer is greater when the hot plate is at the bottom rather than at the top. Thermal rectification is beneficial in two broad situations:

(A) The direction of the heat flux changes with time. This is sometimes the case for thermal barrier coatings, for example on aircraft or when mounting an optoelectronic device to a substrate with transient fluctuations. If the substrate is hotter than the device, the device should be protected by thermal insulation; but if the device becomes hotter than the substrate, the mounting material should become a thermal conductor to maximize heat dissipation.

Focusing on power generation, one can imagine a full-wave, H-bridge, solar-thermal rectifier (Fig. 2). Particularly in desert climates, the nighttime sky temperature is much colder than the ground, and so can be exploited as a heat sink for radiation. The solar-thermal rectifier would convert the daily oscillating "AC" temperatures into an almost-constant "DC" temperature, which powers a heat engine continuously, even in the dead of the night. Compared to a conventional solar-thermal power plant [8,9], this scheme could improve the efficiency (by lowering T_C) and also the duty cycle (by generating at night).

(B) There is some other desirable flux in the opposite direction as the heat flow. In thermoelectric refrigeration [10], the phonons travel in the opposite direction as the majority carriers (electrons in n-leg, holes in p-leg). Thus, if each leg is a ballistic rectifier of both phonons and majority carriers, we can achieve the desirable situation where the phonons are "reverse biased" (lowering the thermal conductivity), while the majority carriers are "forward biased" (preserving the electrical

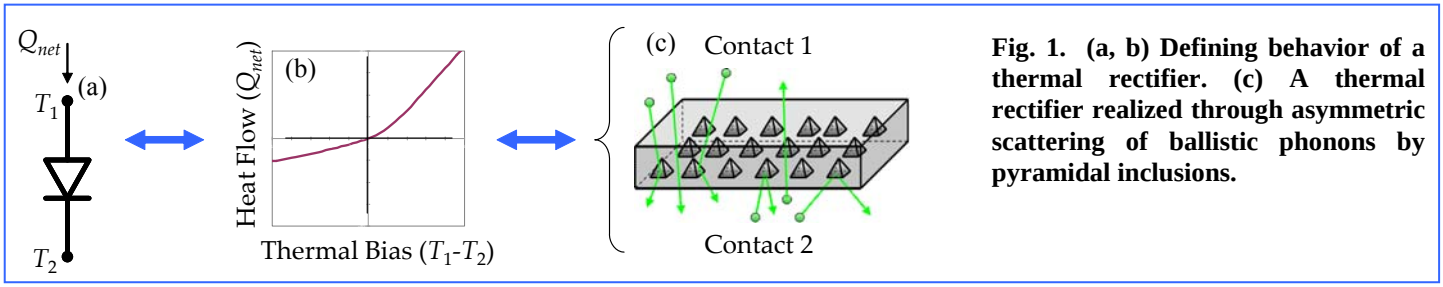

Fig. 1. (a, b) Defining behavior of a thermal rectifier. (c) A thermal rectifier realized through asymmetric scattering of ballistic phonons by pyramidal inclusions.

conductivity) [11,12]. These two effects increase the thermoelectric figure of merit, ZT, and improve the efficiency.

2. BACKGROUND ON THERMAL RECTIFICATION

2.1. MECHANISMS OF THERMAL RECTIFICATION: ASYMMETRY + NONLINEARITY

The thermal rectification, γ, can be defined as

$$\gamma(T_H, T_C) = (Q_{Fwd} - Q_{Rev}) / Q_{Rev}, \qquad (1)$$

where Q_{Fwd} and Q_{Rev} are the heat flows when the temperature difference T_H -T_C is applied in "forward thermal bias" and "reverse thermal bias," respectively. Every thermal rectifier must have an *asymmetry* and a *non-linearity*. At the *macroscale*, solid-state thermal rectification is possible even within the framework of classical heat conduction by Fourier's Law, in a simple two-segment bar if the thermal conductivities of the segments have different dependencies on temperature [13-17]. Other mechanisms have been reviewed by Walker [18], including the effect of thermal expansion on the contact resistance between two adjacent surfaces [18,19], although this effect is harder to control.

Studies of thermal rectification at the *microscale* began in earnest in 2002. From the modeling perspective, other than the ballistic-elastic approach (described next), most efforts focused on detailed atomistic calculations for one-dimensional chains with idealized potentials, often with two different segments [15,20-25]. To date, the only experimental report of microscale thermal rectification was γ up to 7% in individual nanotubes with asymmetric mass loading, a result which was tentatively attributed to solitons but is not well-understood [26].

2.2 THE BALLISTIC-ELASTIC RECTIFICATION MECHANISM

In contrast to the one-dimensional chain approaches, in this work we focus on the asymmetric scattering of ballistic phonons, closely related [11,12]. Compared to the idealized 1-dimensional chain approaches, this mechanism has much better potential to be realized in practical systems. The essential idea

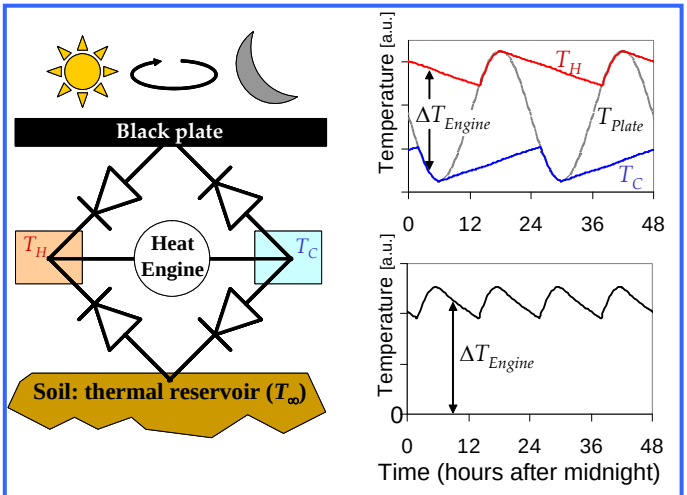

Fig. 2. A full-wave solar-thermal rectifier. The daily temperature oscillations of the black plate are rectified into a nearly-constant Δ*T* across the engine, day and night (preliminary calculations).

is depicted in Fig. 1(c), for a thin film with pyramidal inclusions. (Many other asymmetric nanostructures are also available; see Fig. 3.) Referring to Fig. 1(c), phonons with near-vertical trajectories emitted from the top contact have a high probability of transmission, while phonons emitted from the bottom contact have a high probability of being backscattered. Thus we expect heat flow to be "easy" from top to bottom, but "difficult" from bottom to top. However, this argument is dangerous because it also seems to suggest that there will be spontaneous separation of energy carriers into hot and cold populations, even if we begin from uniform thermodynamic equilibrium, which would violate the 2nd Law of Thermodynamics. As outlined below, careful consideration of the ballistic mechanism reveals that this is not the case.

A related mechanism of ballistic-elastic rectification was previously shown experimentally by Song *et al.* in a two-dimensional electron gas, for the flow of *electrical current*, not *heat* [6,7]. In other related work, Krishnan *et al.* studied the asymmetric transmission of collimated acoustic waves [27], although did not analyze the thermodynamics or heat transport. A preliminary analysis of ballistic thermal rectification of phonons in a sawtooth nanowire was given by Saha, Shi, and

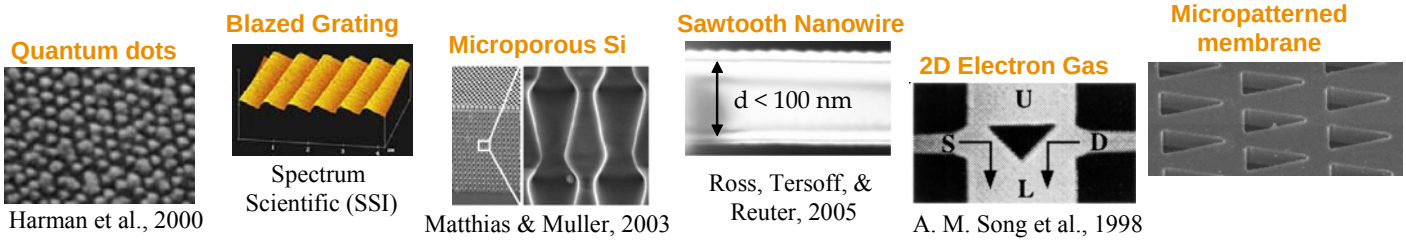

Fig. 3. Various asymmetric nanostructures which could be used for thermal rectification. Refs. [1-7]

Prasher [11,12], and similarly, Roberts and Walker have also considered asymmetric transport in a model system with direction-dependent specularity [28]. However, as detailed below it appears that the common assumption of quasi-equilibrium reservoirs (like blackbody boundary conditions) turns out, surprisingly, to be too simplified for the problem at hand.

3. MODELING RESULTS

3.1. MODELING APPROACH: LANDAUER-BÜTTIKER FORMALISM

We begin with the generalized two-terminal device shown in Fig. 4(a). Many asymmetries are possible, including the reflections from device sidewalls [11,12,28] and contacts, scattering by inclusions or defects, and interfaces between layers. Coherent interference phenomena (filters, speckle, and localization) are also permitted. Because each individual trajectory is reversible, the device satisfies the principle of detailed balance [29,30].

The standard approach to model ballistic transport

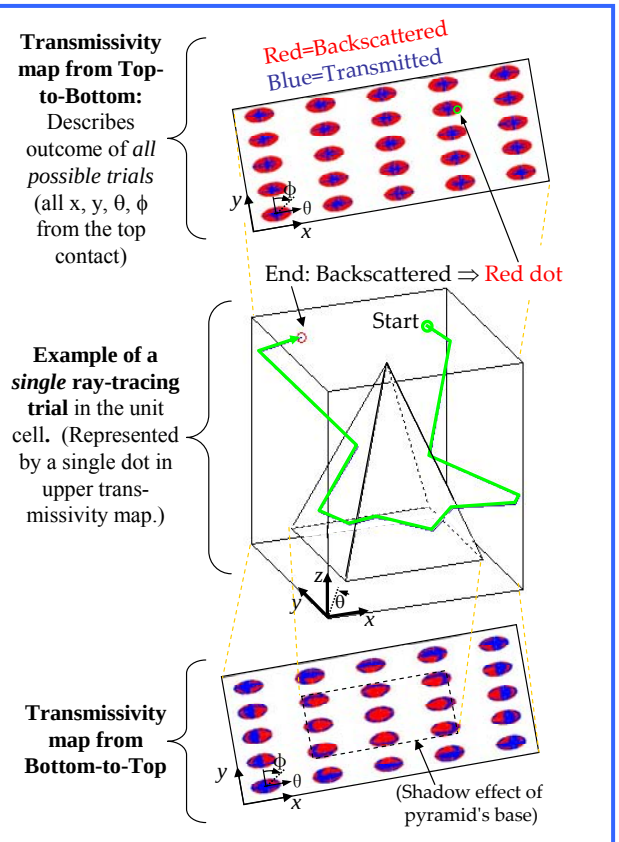

Fig. 4. Ray tracing analysis of particle trajectories for a single layer of pyramidal inclusions. The simulation domain is a unit cell, with specular-reflecting sidewalls due to symmetry.

through a two-terminal device is the Landauer-Büttiker formalism [31-35]. Each contact is a large reservoir which emits and absorbs phonons. Every phonon that enters the device is ultimately either transmitted to the opposite reservoir, or backscattered to its original reservoir. The work presented here is limited to purely elastic scattering, which assumes that the characteristic device dimensions are much smaller than the inelastic mean free path of the phonons [34].

Within this ballistic-elastic framework, the system geometry can be fully described by t_{12} and t_{21}, the transmission probabilities for particles incident on the system from a reservoir. Each transmission function may depend on the location (x,y) and angle (θ,ϕ) of emission. For simplicity we neglect the effects of polarization (p) and wavelength (λ) on t_{12} and t_{21}.

When the reservoirs are out of thermal equilibrium, the net heat flow is given by the difference of the dynamic currents from 1→2 and 2→1. Thus, $Q = Q_{12} - Q_{21}$. Each dynamic current is calculated from the statistics of the incident carriers multiplied by the system transmission function. For example,

$$Q_{12} = \frac{1}{8\pi^3} \sum_p \int_{\mathbf{k}} \int_{\mathbf{x}_1} t_{12} \hbar\omega \, f_1 \; \mathbf{v} \cdot \mathbf{n}_1 \; d^2\mathbf{x}_1 \, d^3\mathbf{k} \,, \qquad (2)$$

and similarly for Q_{21}. Here $\mathbf{k}$ is the wavevector, $\mathbf{v}(\mathbf{k},p)$ is the group velocity, $\mathbf{n}_1(\mathbf{x}_1)$ is the local unit normal of the contact

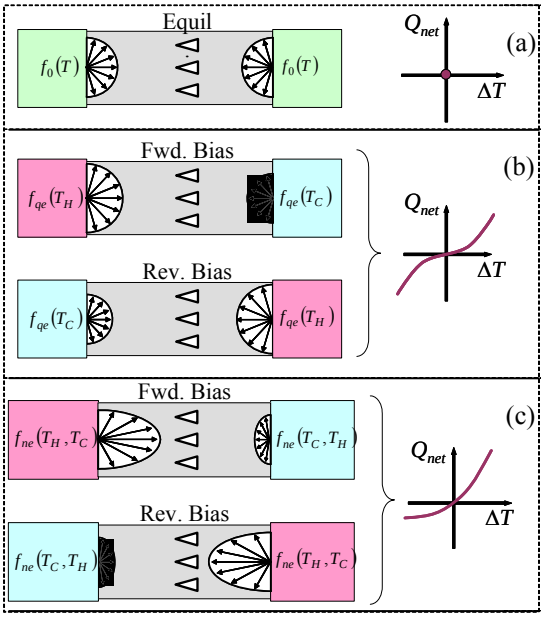

Fig. 5. Net heat flow through a ballistic thermal rectifier. (a) Equilibrium: The 2nd Law requires Q_{net}=0. (b) Quasi-equilibrium reservoirs: transport is symmetric, thus no rectification. (c) Distorted distribution functions: Ballistic rectification is now possible.

surface, and f_1 is the distribution function within reservoir 1 near the contact.

3.2. CONSTRAINTS OF THE 2ND LAW OF THERMODYNAMICS

At thermal equilibrium, Q=0 and T_1=T_2=T. See Fig. 5(a). In this case we showed [36] that

$$Q(T_H,T_C)=0=\int_\omega \left[H_1(\omega)-H_2(\omega)\right]f_0(\omega,T)d\omega\,, \qquad (3)$$

where f_0 is the equilibrium distribution function, and the spectral transmission function [22,33,37] is

$$H_1(\omega)=\tfrac{1}{8\pi^3}\sum\nolimits_p\int_{\theta,\phi,\mathbf{x}_1} t_{12}\hbar\omega\,\mathbf{v}\cdot\mathbf{n}_1\; d^2\mathbf{x}_1\,k^2\sin\theta d\theta d\phi/\,\mathbf{v}\cdot\hat{\mathbf{k}} \qquad (4)$$

with a similar expression for H_2 upon exchanging the indices 1↔2. The key observation in Eq. (3) is that f_0 gives different weightings to different ω as temperature varies. Thus, for Eq. (3) to hold at any arbitrary temperature, we must have

$$H_1(\omega)=H_2(\omega)=H(\omega) \qquad (5)$$

at every ω. Regardless of the geometry of the device, which determines t_{12} and t_{21}, we find that H_1(ω) and H_2(ω) will always be equal. Thus, the geometric quantities t_{12} and t_{21} are coupled by the thermodynamic constraints of Eqs. (4) and (5). This major constraint is a new result, and applies to all types of energy carriers at all temperatures, including at non-equilibrium.

We now return to a non-equilibrium condition when T_1 is hot and T_2 is cold. Most of the previous approaches to study thermal transport in the Landauer-Büttiker formalism invoke the assumption of quasi-equilibrium reservoirs (i.e., a thermal bath approach) [11,12,20-25,32,33,37-39], whereby the outward-going portion of f is approximated by the quasi-equilibrium distribution function corresponding to the local reservoir temperature. That is, we usually assume $f_1(\mathbf{x}_1,\theta,\phi,\omega,p)\approx f_0(\omega,T_1)$, as shown in Fig. 5(b). This is equivalent to the assumption of black plates in radiation heat transfer, or the two-flux method, i.e., S_2 or Schuster-Swarzchild approximation [40-42]. For photons and phonons, f_{qe} is the Bose-Einstein function, $\left[\exp\left(\hbar\omega/k_BT_1\right)-1\right]^{-1}$.

However, according to the assumption of quasi-equilibrium reservoirs, from Eqs. (3) and (5) we have

$$Q(T_H,T_C)=\int_\omega \left[f_{qe}(\omega,T_H)-f_{qe}(\omega,T_C)\right]H(\omega)d\omega\,.$$

But if the temperatures of the contacts are reversed, we see that this simply changes the sign of the resulting heat flux, without changing its magnitude. That is, the Q vs. ΔT curve is symmetric: $Q(T_C,T_H)$ = $-Q(T_H,T_C)$. Thus, the standard Landauer-Büttiker approach using two reservoirs each in local quasi-equilibrium is incapable of modeling thermal rectification by the ballistic-elastic mechanism. To model rectification, it is essential to incorporate the distortions of the emitted portions of the distribution function at non-equilibrium. We have confirmed this important result (the failure of the quasi-equilibrium assumption to give rectification) by applying blackbody boundary conditions to t_{12} and t_{21} calculated for various geometries including quantum dots and sawtooth nanowires of various shapes and sizes. Furthermore, for diffuse scatterers this result is evident from classical radiation view factor analysis (with black or gray boundaries, Q is always symmetric in $\sigma T_1^4-\sigma T_2^4$, [40,41]). It has also been observed in Monte Carlo simulations of enclosures with various geometries and specularities [43].

3.3. A DISTORTED BOUNDARY CONDITION: THE DISPLACED BOSE-EINSTEIN DISTRIBUTION

Some degree of distortion must always be present whenever there is net transport. The mathematical reason is simply that the net heat flux in bulk (an expression similar to Eq. (2) with t_{12}=1) vanishes if f is symmetric about **k=0** [44,45]. The physical reason is shown in Fig. 6(a). Consider phonons diffusing through a solid with a temperature gradient. At a particular location $\boldsymbol{x}$, the forward-going part of the distribution function is made up of phonons that had their most

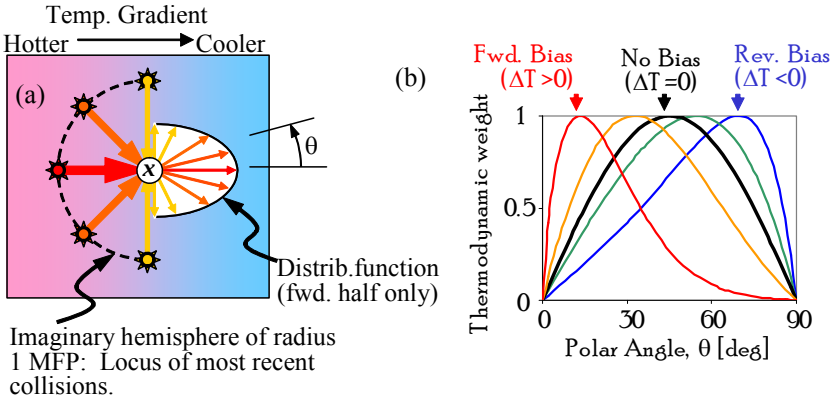

Fig. 6. (a) Physical reason for the distorted distribution function when there is diffusive transport: the carriers at a position x arrive from different locations with different local T. (b) Thermodynamic weight w(θ) for several values of thermal bias (u_0=-4, -2, ... 4), from the displaced Bose-Einstein approximation. Each curve is normalized.

recent collisions a distance of one mean-free-path (MFP) away. Thus, the phonons traveling in direction θ=0° came from the hottest region, while the phonons traveling in direction θ=45° arrive with "cooler" characteristic energy, and the phonons in θ=90° are cooler still. To a rough approximation, the dimensionless magnitude of the distortions in the bulk phase are of the order $(\Lambda \nabla T)/T$, where Λ is the mean free path, and ∇T is the gradient of the local average absolute temperature T. Although usually safely neglected, these distortions are always important for steep temperature gradients and long MFPs, and must in fact be maximized for ballistic rectification. We desire, then, to have an inelastic, diffusive region (Fig. 6a) at each contact, to distort the distributions before they are emitted into the ballistic-elastic portion of the device (the gray region in Fig. 4).

These distortions can be approximated using a drifted Bose-Einstein distribution [46,47], analogous to the drifted Maxwellian used in electron modeling [48,49]. The non-equilibrium distribution function f_{ne} is assumed equivalent to an equilibrium distribution centered on a displaced wavevector $\mathbf{k}_0$, that is, $f_{ne} = \left[\exp\left(\hbar\omega(\mathbf{k}-\mathbf{k}_0)/k_B T\right)-1\right]^{-1}$. For simplicity we focus on the low-temperature, isotropic Debye limit, and plane-parallel contacts. We showed [50,51] that the drift wavevector is directly proportional to the heat flux vector $\mathbf{q}$ within the diffusive reservoir, $\mathbf{k}_0 = \pi^2\hbar^2 c\,\mathbf{q}/3\zeta(3)k_B^3 T^3$, where ζ(3)=1.202... is Apéry's constant, and c is the average sound velocity. In this limit we find $Q_{12} = q_0 \int_{\theta,\phi,\mathbf{x}_1} t_{12}\, w\, d\theta\, d\phi\, d^2\mathbf{x}_1$, where $q_0 = 3k_B^4 T_1^4/8\pi^3 c^2\hbar^3$ is the characteristic heat flux scale, and the dimensionless weighting factor is

$$w(\theta,u_0) = \sin\theta\cos\theta \times \int_0^{u_{\max}} u^3 \left[\exp\left(\sqrt{u^2+u_0^2-2uu_0\cos\theta}\right)-1\right]^{-1} du \qquad (6)$$

where $u_0 = \hbar c|\mathbf{k}_0|/k_B T$ is a dimensionless "distortion parameter" or dimensionless "thermal bias." This weighting factor is shown in Fig. 6(b). It is like the intensity of Fig. 6(a), multiplied by sin(θ) (differential solid angle effect) and cos(θ) (projected area effect). The key is that forward thermal bias places more weight on θ~0° and less on θ~90°.

3.4. VALIDATION: COMPARISON WITH ANALYTICAL RESULT FOR A NANO-WIRE

To validate the Landauer / distorted Bose-Einstein approach described above, we used the same methods to calculate the thermal conductivity of a square nanowire, a system which has a well-known analytical solution. We considered nano-wires 100 nm x 100 nm square in cross section, with completely diffuse side walls, and lengths ranging from 10 nm to 5 μm. Our ray-tracing Landauer approach was used to calculate the net heat transfer, Q_{net}, as a function of the temperature gradients. We then compared the computer models' calculations to an analytical model, beginning with a simple Fourier analysis

$$Q_{net} = -kA\frac{dT}{dx}$$

where k is the thermal conductivity, A is the cross sectional area, and dT/dx is the temperature gradient. From kinetic theory,

$$k = \frac{1}{3}Cv\Lambda$$

where C is the specific heat, v is the mean phonon velocity, and Λ is the phonon mean free path. For a square nanowire of side 100 nm, in the limit of strong boundary scattering, Λ=112 nm [52]. Focusing on the low-temperature Debye limit and low thermal bias, the Debye specific heat can be expressed as

$$C = \frac{16T_{ave}^3\sigma}{v}$$

where T_{ave} is the average temperature of the device and σ is the material-dependent phonon Stefan-Boltzmann constant. By combining these models together we obtain

$$Q_{net} = -\frac{16}{3}T_{ave}^3\sigma\Lambda A\frac{dT}{dx}$$

This analytical result (red lines) is compared to our Landauer / Bose-Einstein calculations (blue lines) at 10 K in Fig. 7. As expected, the agreement between the two methods is excellent at low thermal bias (linear regime).

3.5. PHONON RECTIFICATION BY PYRAMIDAL VOIDS

Having verified the basic accuracy of our Landauer method, we used phonon ray tracing (Fig. 8a) to study the structure of Fig. 1(c) [50,51]. The pyramids are specularly-reflecting voids (height : base = 2:1, and 50% coverage by projected area) and all other scattering mechanisms were neglected. Typical transfer functions are shown as "dot plots" in Fig. 8(b,d), for a unit cell with a single pyramidal inclusion. Each tiny dot is the result of a single (x,y,θ,ϕ) ray-tracing trial. The 25 subplots are organized in an x,y grid, corresponding to a 5 x 5 mesh of x,y launch locations. Within a single subplot, the polar location of each dot corresponds to its θ,ϕ launch direction (mesh of ~500 θ,ϕ pairs per subplot). For particles launched from the bottom (Fig. 8d), the shadowing effect of the pyramid's base appears as the red region of zero transmissivity near the center of the plot.

After averaging over x, y, and azimuthal angle ϕ, the particle transmission as a function of polar angle θ is shown in

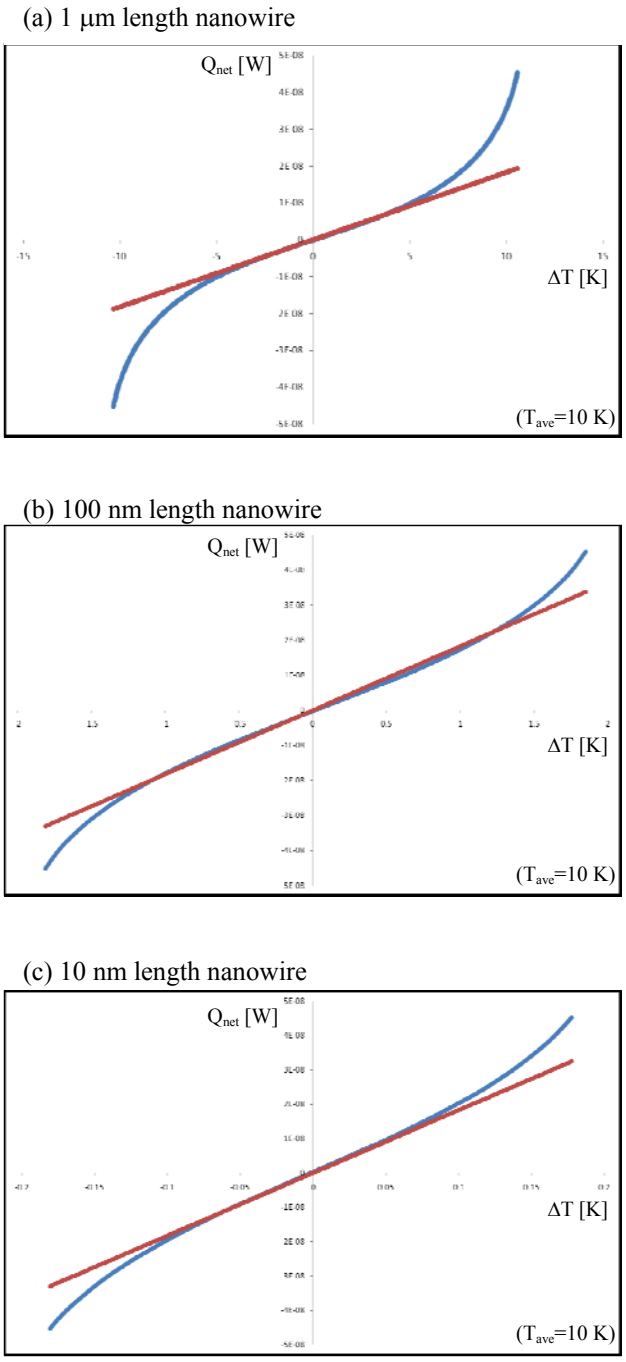

Fig. 7. Calculated thermal transport in square nanowires of three different lengths. Blue lines: Landauer formalism with distorted Bose-Einstein boundary condition (present work). Red lines: linearized analytical result of Fourier's law using an effective thermal conductivity found from simple kinetic theory.

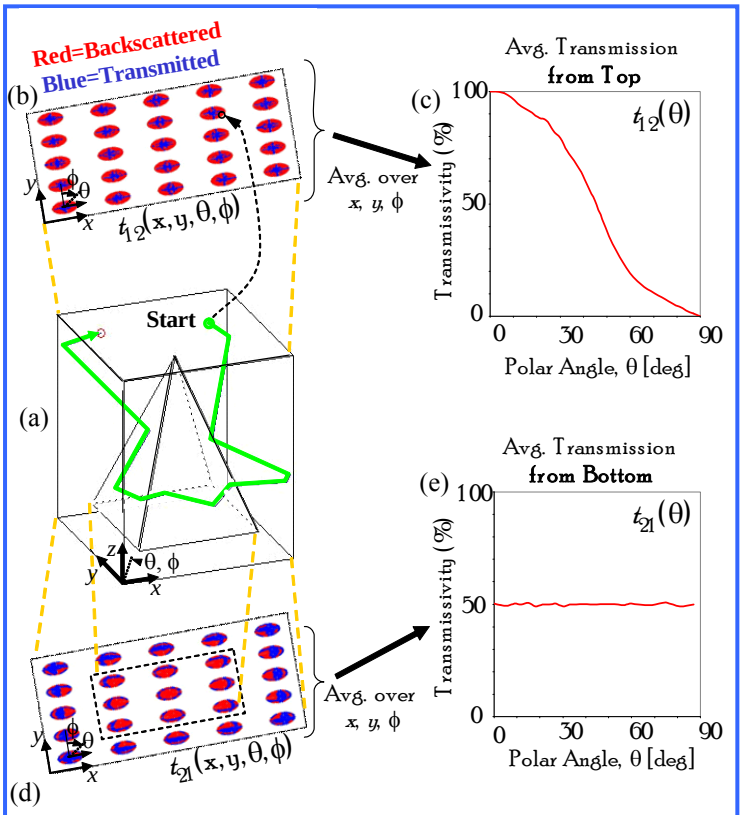

Fig. 8. Determining transmissivities by phonon ray tracing. (a) A particular trajectory for emission from the upper contact. (b) A 4-dimensional transmissivity map for $t_{12}(x,y,\theta,\phi)$. The trajectory from part (a) is the single red dot indicated by the dashed arrow. (c) Focusing on the θ-dependence of $t_{12}(\theta)$. (d) Map for t_{21}, showing strong backscattering (red) underneath the pyramid's base. (e) In contrast to $t_{12}(\theta)$, the average θ-dependence of t_{21} is nearly constant.

Fig. 8c,e. For transport from top-to-bottom (Fig. 8c), small-θ particles are almost all transmitted, while in the opposite direction (Fig. 7e), small-θ particles are 50% backscattered. This is the other key to thermal rectification: $t_{12}(\theta)$ and $t_{21}(\theta)$ should have opposite trends in θ. This also resolves the 2nd Law paradox mentioned in the Introduction: Although t_{12} may be large for θ~0°, the necessary penalty is that t_{12} is much lower for θ~90°.

Finally, the calculated heat flows are shown in Fig. 9. The calculation satisfies the 2nd Law of Thermodynamics, because at thermal equilibrium (zero bias), $Q_{12}=Q_{21}$ and there is no net heat transfer. More importantly, thermal rectification is clearly present, with γ approaching 73% for a thermal bias of 4.

Diffuse vs. specular scattering. Although the transmissivity maps of Fig. 7(b,d) assumed purely specular scattering, diffuse scattering becomes important once the surface roughness exceeds ~1/10 of the phonon wavelength (Ziman's specularity p [44,53]), and deterministic ray tracing breaks down. Using a Monte Carlo method, simulations show

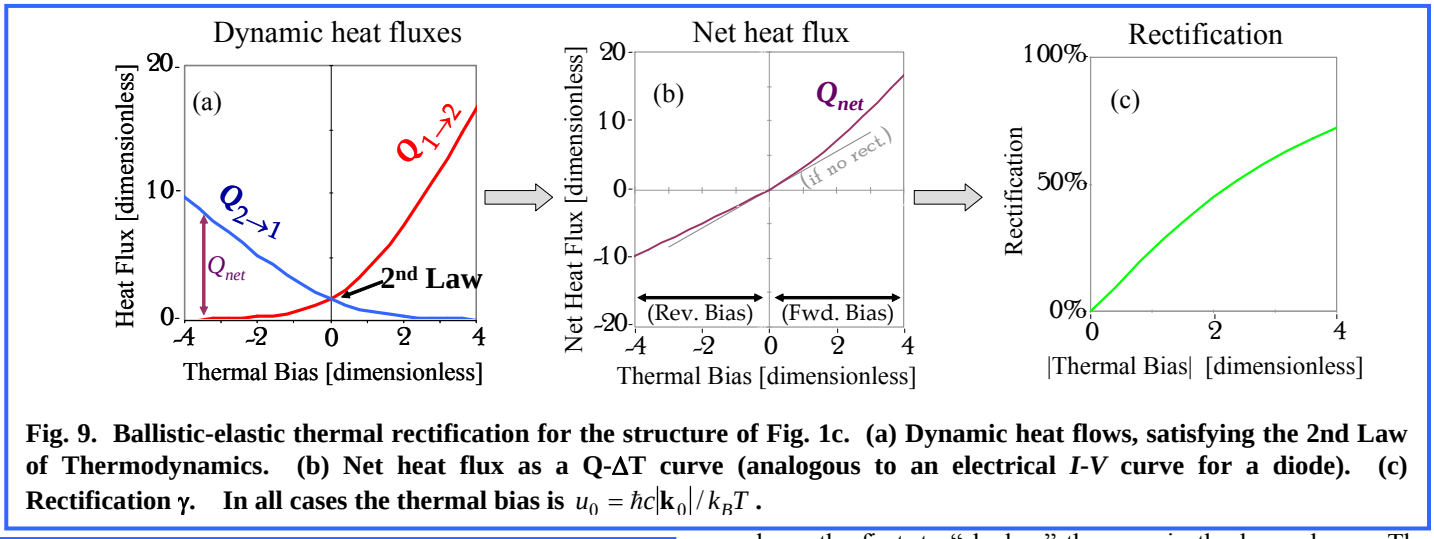

Fig. 9. Ballistic-elastic thermal rectification for the structure of Fig. 1c. (a) Dynamic heat flows, satisfying the 2nd Law of Thermodynamics. (b) Net heat flux as a Q-ΔT curve (analogous to an electrical *I-V* curve for a diode). (c) Rectification γ. In all cases the thermal bias is $u_0 = \hbar c|\mathbf{k}_0|/k_B T$.

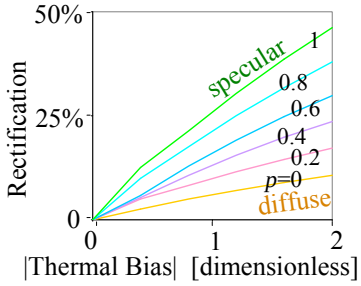

Fig. 10. Monte Carlo analysis of the effect of specularity on rectification. Compare to Fig. 9(c).

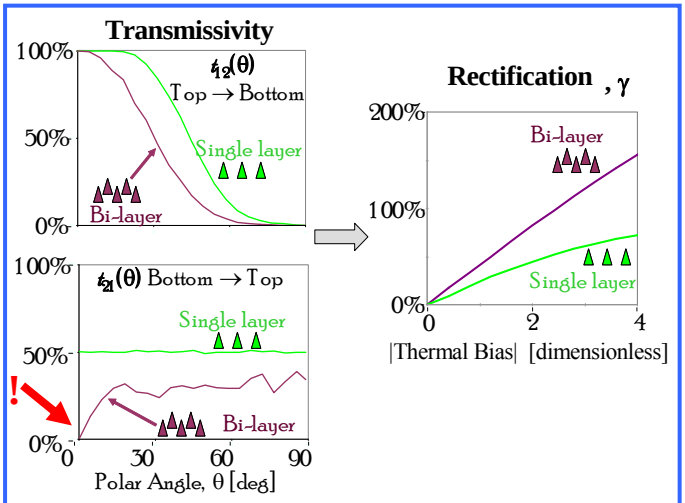

Fig. 11. Effect of adding a 2nd layer of pyramidal scatterers. The transmissivity in reverse bias direction, $t_{21}(\theta)$, now shows a null at θ=0, resulting in stronger rectification.

that rectification is still possible even for purely diffuse scattering at the inclusion surfaces (Fig. 10).

Multilayer arrays of pyramidal inclusions. As shown in Figs. 1c and 7, in the present structure 50% of the phonons emitted from the bottom contact pass through the structure. Intuition suggests adding a second layer of pyramids staggered above the first, to "shadow" the gaps in the lower layer. The results of this calculation are shown in Fig. 11. The key is that $t_{21}(\theta)$ for the bi-layer structure now goes to zero as $\theta \to 0°$, in contrast to the constant value of $t_{21}(\theta)$ for the single-layer structure. Because the bi-layer structure now exhibits stronger contrast in $t_{12}(\theta)$ vs. $t_{21}(\theta)$, we expect greater rectification, as confirmed in Fig. 11. (Note that values of γ>100% are permitted by the definition in Eq. (1): Just like an electrical diode, there is no natural upper limit on the rectification).

4. POSSIBLE EXPERIMENTS

The above theoretical results suggest that the ballistic-elastic rectification mechanism may permit structures with the capacity for large thermal rectification. We now briefly describe two experimental systems which might be used to realize this effect.

4.1. PHONONS IN ASYMMETRIC SI MEMBRANES

Structures like that shown in Fig. 12 could be used to directly measure the performance of a single rectifier in both forward and reverse bias. For example, when Q_1 is powered with Q_2=0, the diode region is forward biased, and when Q_2 is powered with Q_1=0, the diode region is reverse biased. The device in Fig. 12(a-c) has a single rectification region in its center, and is prepared from a silicon-on-insulator (SOI) wafer by standard microfabrication techniques, similar to the demonstration device in Fig. 12d. Related structures could be prepared with a variety of different shapes of the asymmetric scatterers, their aspect ratio, the number of rows, etc. The fabrication parameters can also be varied [54] to quantify the effect of sidewall roughness on specularity and rectification.

4.2. PHOTONS BETWEEN BLACKBODIES

A second possible experiment is shown in Fig. 13. Two blackbody cavities [40,41] are used to drive radiation heat

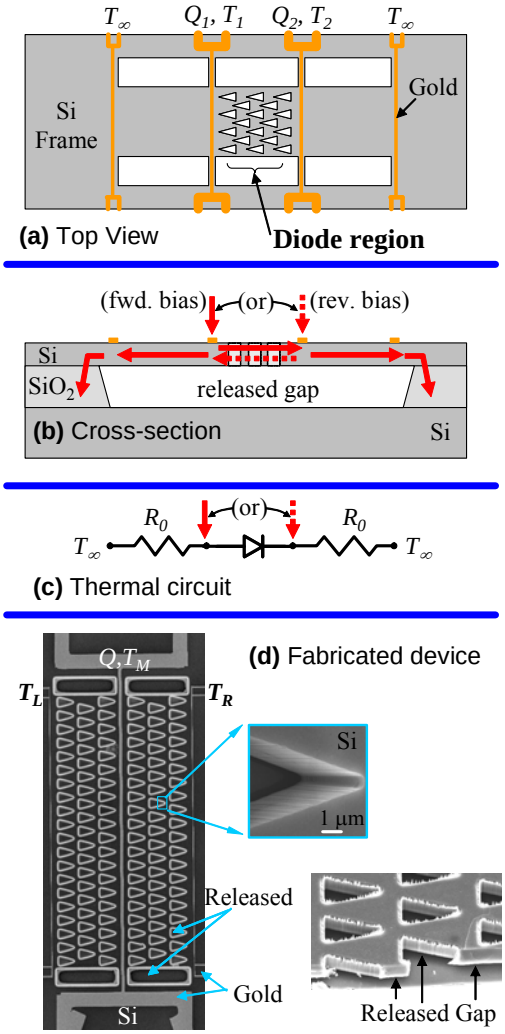

Fig. 12. Experiment E1: Rectification of phonons by asymmetric microfabricated pores.

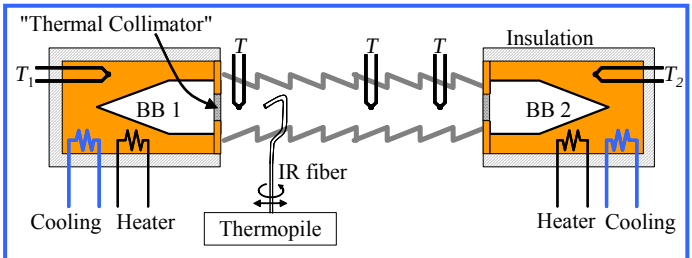

Fig. 13. Asymmetric photon transport between two blackbodies along a thermal rectification test section with sawtooth mirrors. (Nanowire analogy)

transfer along a ballistic-elastic thermal rectification test section with asymmetric reflectors. The diode response is readily determined by measuring the Q vs. ΔT curve for the test section. This system is an analogue of the classical ballistic size effect on phonons/electrons in an asymmetric nanowire, but in a more flexible configuration. The rectifier test section could be made of asymmetric mirrors, blazed diffraction gratings, *etc.*, coated with a broadband infrared (IR) reflector such as silver or gold. The aperture of each cavity can include an interchangeable thermal collimator window, allowing the study of the effectiveness of many different collimation strategies (e.g., aligned cylinders (capillary tubes). a randomly etched diffuser of IR-transparent CaF_2, or thin layers of carbon black or soot (IR absorbtion length ~100 μm[40,41]) deposited directly on a CaF_2 window.)

The experiment of Fig. 13 complements that of Fig. 12 because the mirrors in Fig. 13 can easily be made highly specular. Another benefit of studying this photon rectifier is that such devices can in principle be scaled down using microfabrication or self-assembled nanomaterials (e.g. opaque quantum dots in a transparent matrix), and might eventually prove useful for thermal-photovoltaic (TPV) power generation.

5. SUMMARY

In summary, we have described the fundamental principles and limitations of ballistic-elastic thermal rectification. These general principles apply for all types of energy carriers in elastic asymmetric scattering. The 2nd Law of Thermodynamics imposes an integral constraint on the geometric transmission functions t_{12} and t_{21}, and also shows that the common assumption of quasi-local-equilibrium thermal reservoirs is insufficient capture ballistic-elastic thermal rectification. Instead, it is essential to account for the *distortions* of the emitted distribution function, for example using a displaced Bose-Einstein distribution. We note that these distortions could be further increased by the use of anisotropic materials in the reservoirs. The other key ingredient for ballistic elastic thermal rectification is that the averaged transmissivities $t_{12}^{\theta}(\theta)$ and $t_{21}^{\theta}(\theta)$ should have opposite trends. Specifically, t_{12}^{θ} should increase for $\theta=\pi/2\rightarrow 0$, while t_{21}^{θ} should decrease for $\theta=\pi/2\rightarrow 0$ (Fig. 11a,b). These results point the way towards rational optimization of the asymmetric geometries, as illustrated by the increased rectification effect by adding a second layer of scatterers (Fig. 11c). Finally, this phenomenon should be experimentally accessible in a variety of systems, such as phonons in nanostructured solids, or photon radiation through a cavity with asymmetric mirrors.

ACKNOWLEDGMENTS

We thank Greg Walker, Li Shi, Rama Venkatasubramanian, and Joe Mantese for stimulating discussions. This work is supported in part by the DARPA/DSO NMP program (W911NF-08-C-0058).

REFERENCES

1. T. C. Harman, P. J. Taylor, D. L. Spears, and M. P. Walsh, "Thermoelectric quantum-dot superlattices with high ZT". *Journal of Electronic Materials* **29**, L1-L4 (2000).
2. Y. Fujii, K. I. Aoyama, and J. I. Minowa, "OPTICAL DEMULTIPLEXER USING A SILICON ECHELETTE GRATING". *Ieee Journal of Quantum Electronics* **16**, 165-169 (1980).
3. S. Matthias and F. Muller, "Asymmetric pores in a silicon membrane acting as massively parallel brownian ratchets". *Nature* **424**, 53-57 (2003).
4. F. M. Ross, J. Tersoff, and M. C. Reuter, "Sawtooth Faceting in Silicon Nanowires". *Physical Review Letters* **95**, 146104-146104 (2005).
5. H. Peng, S. Meister, C. K. Chan, X. F. Zhang, and Y. Cui, "Morphology Control of Layer-Structured Gallium Selenide Nanowires". *Nano Lett.* **7**, 199-203 (2007).
6. A. M. Song, A. Lorke, A. Kriele, J. P. Kotthaus, W. Wegscheider, and M. Bichler, "Nonlinear electron transport in an asymmetric microjunction: A ballistic rectifier". *Physical Review Letters* **80**, 3831-3834 (1998).
7. A. M. Song, "Formalism of nonlinear transport in mesoscopic conductors". *Physical Review B* **59**, 9806 (1999).
8. J. W. Tester, E. M. Drake, M. J. Driscoll, M. W. Golay, and W. A. Peters, *Sustainable Energy: Choosing among options*. (MIT Press, 2005).
9. U. Herrmann and D. W. Kearney, "Survey of thermal energy storage for parabolic trough power plants". *J. Sol. Energy Eng. Trans.-ASME* **124**, 145-152 (2002).
10. G. S. Nolas, J. Sharp, and H. J. Goldsmid, *Thermoelectrics: basic principles and new materials developments*. (Springer-Verlag, New York, 2001).
11. S. Saha, L. Shi, and R. Prasher, presented at the ASME Int. Mech. Eng. Congr. Exp., Chicago, 2006 (unpublished).
12. S. Saha, Ph.D. thesis, University of Texas, Austin, 2007.
13. C. Dames, "Solid-state thermal rectification with existing bulk materials". *Journal of Heat Transfer (in review)* (2008).
14. K. Balcerek and T. Tyc, "Heat flux rectification in tin-alpha-brass system". *Physica Status Solidi (a)* **47**, K125-K128 (1978).
15. M. Peyrard, "The design of a thermal rectifier". *EPL (Europhysics Letters)* **76**, 49-55 (2006).
16. Heinrich Hoff, "Asymmetrical heat conduction in inhomogeneous materials". *Physica A: Statistical and Theoretical Physics* **131**, 449-464 (1985).
17. Heinrich Hoff and Paul Jung, "Experimental observation of asymmetrical heat conduction". *Physica A: Statistical Mechanics and its Applications* **199**, 502-516 (1993).
18. D. G. Walker, presented at the Joint ASME-ISHMT Heat Transfer Conference, Guwahati, India, 2006 (unpublished).
19. A. M. Clausing, "Heat transfer at the interface of dissimilar metals--the influence of thermal strain". *International Journal of Heat and Mass Transfer* **9**, 791-801 (1966).
20. M. Terraneo, M. Peyrard, and G. Casati, "Controlling the Energy Flow in Nonlinear Lattices: A Model for a Thermal Rectifier". *Physical Review Letters* **88**, 094302 (2002).
21. Baowen Li, Lei Wang, and Giulio Casati, "Thermal Diode: Rectification of Heat Flux". *Physical Review Letters* **93**, 184301-184304 (2004).
22. Dvira Segal and Abraham Nitzan, "Spin-Boson Thermal Rectifier". *Physical Review Letters* **94**, 034301-034304 (2005).
23. Jean-Pierre Eckmann and Carlos Mejia-Monasterio, "Thermal Rectification in Billiardlike Systems". *Physical Review Letters* **97**, 094301-094304 (2006).
24. B. Hu, D. He, L. Yang, and Y. Zhang, "Thermal rectifying effect in macroscopic size". *Physical Review E (Statistical, Nonlinear, and Soft Matter Physics)* **74**, 060201-060204 (2006).
25. Y. Ming, Z. X. Wang, Q. Li, and Z. J. Ding, "Nonlinear thermal properties of three-terminal mesoscopic dielectric systems". *Applied Physics Letters* **91**, 143508-143503 (2007).
26. C. W. Chang, D. Okawa, A. Majumdar, and A. Zettl, "Solid-state thermal rectifier". *Science* **314**, 1121-1124 (2006).
27. R. Krishnan, S. Shirota, Y. Tanaka, and N. Nishiguchi, "High-efficient acoustic wave rectifier". *Solid State Communications* **144**, 194-197 (2007).
28. D. G. Walker, unpublished work (2007).
29. Richard C. Tolman, "The Principle of Microscopic Reversibility". *Proceedings of the National Academy of Sciences of the United States of America* **11**, 436-439 (1925).
30. F. Reif, *Fundamentals of statistical and thermal physics*. (McGraw-Hill, Boston, MA, 1965).
31. R. Landauer, "SPATIAL VARIATION OF CURRENTS AND FIELDS DUE TO LOCALIZED SCATTERERS IN METALLIC CONDUCTION". *Ibm Journal of Research and Development* **1**, 223-231 (1957).
32. Luis G. C. Rego and George Kirczenow, "Quantized Thermal Conductance of Dielectric Quantum Wires". *Physical Review Letters* **81**, 232 (1998).
33. N. Mingo and D. A. Broido, "Carbon nanotube ballistic thermal conductance and its limits". *Physical Review Letters* **95** (2005).
34. S. Datta, *Electronic Transport in Mesoscopic Systems*. (Cambridge Unviersity Press, 1995).

35. Yoseph Imry and Rolf Landauer, "Conductance viewed as transmission". *Reviews of Modern Physics* **71**, S306 (1999).
36. C. Dames, "Thermodynamic constraints on thermal rectification by ballistic-elastic scattering". *in preparation.* (2008).
37. N. Mingo, "Calculation of Si nanowire thermal conductivity using complete phonon dispersion relations". *Physical Review B* **68**, 4 (2003).
38. E. T. Swartz and R. O. Pohl, "THERMAL-BOUNDARY RESISTANCE". *Reviews of Modern Physics* **61**, 605-668 (1989).
39. Francesco Giazotto, Tero T. Heikkila, Arttu Luukanen, Alexander M. Savin, and Jukka P. Pekola, "Opportunities for mesoscopics in thermometry and refrigeration: Physics and applications". *Reviews of Modern Physics* **78**, 217-258 (2006).
40. R. Siegel and J. Howell, *Thermal Radiation Heat Transfer*, 4th ed. (Taylor & Francis, 2001).
41. M. Modest, *Radiative Heat Transfer*, 2nd ed. (Academic Press, 2003).
42. C. Dames and G. Chen, "Theoretical phonon thermal conductivity of Si/Ge superlattice nanowires". *Journal of Applied Physics* **95**, 682-693 (2004).
43. D. G. Walker, simulations using MONT2D, personal communication, 12/14/2007.
44. J. M. Ziman, *Electrons and Phonons*. (Clarendon Press, Oxford, 1960).
45. G. Chen, *Nanoscale Energy Transport and Conversion: A Parallel Treatment of Electrons, Molecules, Phonons, and Photons*. (Oxford University Press, 2005).
46. Joseph Callaway, "Model for Lattice Thermal Conductivity at Low Temperatures". *Physical Review* **113**, 1046 (1959).
47. Sarah Usher and G. P. Srivastava, "Theoretical study of the anharmonic decay of nonequilibrium LO phonons in semiconductor structures". *Physical Review B* **50**, 14179 (1994).
48. M. Lundstrom, *Fundamentals of carrier transport*. (Cambridge University Press, 2000).
49. P. Y. Yu and M. Cardona, *Fundamentals of Semiconductors: Physics and materials properties*, 3rd ed. (Springer, New York, 2005).
50. C. Dames and J. P. Miller, "Thermal rectification by asymmetric scattering of ballistic energy carriers". *In preparation.* (2008).
51. J. P. Miller, W. Y. Jang, and C. Dames, presented at the Energy Nanotechnology International Conference (ENIC), Jacksonville, FL, 2008 (unpublished).
52. H. B. G. Casimir, "Note on the conduction of heat in crystals". *Physica* **5**, 495-500 (1938).
53. Z. M. Zhang, *Nano / Microscale Heat Transfer*. (McGraw-Hill, New York, 2007).
54. K. K. Lee, D. R. Lim, L. C. Kimerling, J. Shin, and F. Cerrina, "Fabrication of ultralow-loss Si/SiO2 waveguides by roughness reduction". *Optics Letters* **26**, 1888-1890 (2001).

.